doi:10.1016/j.jmb.2005.06.029 J. Mol. Biol. (2005) 351, 545–561

JMB

Available online at www.sciencedirect.com

SCIENCE DIRECT®

ELSEVIER

The Structural Basis for Substrate Specificity in DNA Topoisomerase IV

Kevin D. Corbett, Allyn J. Schoeffler, Nathan D. Thomsen and James M. Berger*

Department of Molecular and Cell Biology
237 Hildebrand Hall #3206
University of California Berkeley, Berkeley, CA 94720-3206, USA

**Corresponding author*

Most bacteria possess two type IIA topoisomerases, DNA gyrase and topo IV, that together help manage chromosome integrity and topology. Gyrase primarily introduces negative supercoils into DNA, an activity mediated by the C-terminal domain of its DNA binding subunit (GyrA). Although closely related to gyrase, topo IV preferentially decatenates DNA and relaxes positive supercoils. Here we report the structure of the full-length *Escherichia coli* ParC dimer at 3.0 Å resolution. The N-terminal DNA binding region of ParC is highly similar to that of GyrA, but the ParC dimer adopts a markedly different conformation. The C-terminal domain (CTD) of ParC is revealed to be a degenerate form of the homologous GyrA CTD, and is anchored to the top of the N-terminal domains in a configuration different from that thought to occur in gyrase. Biochemical assays show that the ParC CTD controls the substrate specificity of topo IV, likely by capturing DNA segments of certain crossover geometries. This work delineates strong mechanistic parallels between topo IV and gyrase, while explaining how structural differences between the two enzyme families have led to distinct activity profiles. These findings in turn explain how the structures and functions of bacterial type IIA topoisomerases have evolved to meet specific needs of different bacterial families for the control of chromosome superstructure.

Keywords: β-pinwheel; ATPase; supercoiling; decatenation; DNA binding

Introduction

All organisms invest significant resources toward preserving the informational and structural integrity of their genomes. Many cellular transactions involving DNA, including replication, transcription, and recombination, alter chromosome topology through supercoiling, knotting, and catenation. These structures, when left unresolved, can stall replication and transcription, generate double-strand DNA breaks, or impair the partitioning of replicated DNA to daughter cells[1–6] (Figure 1(a)). Type II topoisomerases circumvent many types of topological problems, transporting one double-helical DNA segment through a transient, enzyme-mediated break in another to modulate DNA superhelicity and unlink tangled chromosomes.[7–9] Due to the importance of these activities, type II topoisomerases are essential for cell viability and are found throughout all cellular domains of life.[10]

Type II topoisomerases (topos) can be placed into two subfamilies based on sequence and structural features. Type IIA topos, the most common class, are found throughout eukaryotes, bacteria, and some archaea. The simpler type IIB topos are restricted to archaea and higher plants.[7,8] Bacterial type IIA topos are A_2B_2 heterotetramers with three subunit interfaces that alternately open and close in response to ATP binding and hydrolysis to effect DNA transport. Their reaction cycle begins when one DNA duplex, termed the "gate" or G-segment, is bound by the A-subunits of the enzyme. Next, a second duplex, termed the "transfer" or T-segment, is captured when the B-subunits bind ATP and dimerize. This event triggers cleavage of the G-segment, and the subsequent hydrolysis of ATP mediates passage of the T-segment through the gap opened in the G-segment. Following transport, the G-segment is resealed and the T-segment is released from the enzyme.

Abbreviations used: CTD, C-terminal domain; NTD, N-terminal domain; topo, topoisomerase; SAD/MAD, single and multi-wavelength anomalous diffraction; CAP, catabolite activator protein.

E-mail address of the corresponding author: jmberger@berkeley.edu

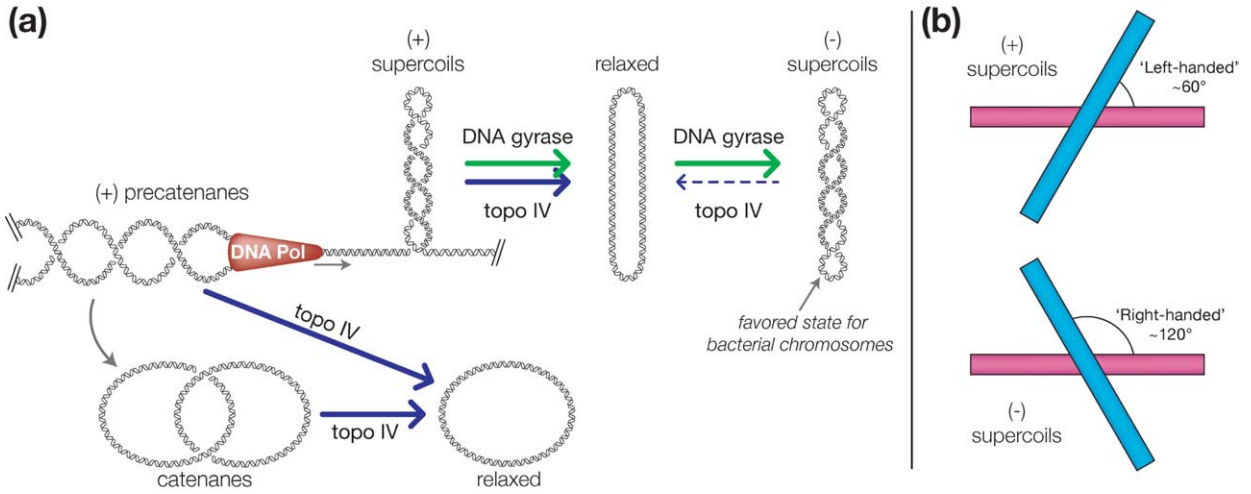

Figure 1. Reactions catalyzed by DNA gyrase and topoisomerase IV. (a) Representative DNA topologies encountered in bacterial cells. Replication produces positive supercoils ahead of the fork and positive-handed precatenanes behind the fork. Unless resolved before replication is complete, precatenanes can become fully linked catenanes. DNA gyrase and topo IV differentially act on these DNA topologies. Gyrase (green arrows) relaxes positive supercoils and introduces negative supercoils to maintain bacterial genomes in a slightly underwound state. Topo IV (blue arrows) removes positive supercoils, catenanes, and knots, and can also relax negative supercoils to a modest extent (dotted arrow). (b) Schematic showing the predominant DNA crossover geometry in positively and negatively supercoiled DNA. "Left-handed" crossovers (crossing angle ~60°) predominate in positively supercoiled DNA, while "right-handed" crossovers occur more often in negatively supercoiled DNA.[36] In considering only local crossover geometry, knowledge of the connectivity between the two segments is unnecessary.

Although this general reaction is common to all type IIA topoisomerases, bacteria have unique requirements that have necessitated further adaptation and specialization of their enzymes. For example, mesophilic bacteria tightly regulate the superhelical density of their genomes to maintain a specific level of negative supercoiling.[11] Negative supercoiling creates strain that favors unwinding of the DNA duplex and is important for many cellular processes that require access to single-stranded DNA, including transcription and the initiation of DNA replication.[12–15] In addition, closed circular bacterial genomes become catenated, or topologically linked, during genome replication, necessitating their separation before cell division.[16,17]

To meet their unique needs, most bacteria possess two specialized type IIA topos (Figure 1(a)): DNA gyrase, encoded by the *gyrA* and *gyrB* genes; and topo IV, encoded by *parC* and *parE*.[18–22] Gyrase catalyzes the formation of negative supercoils and also can relax positive supercoils (a topologically equivalent reaction), but is inefficient at unknotting and decatenation.[23,24] Gyrase's negative supercoiling capability is mediated by a domain at the C terminus of its A-subunit, termed the GyrA CTD, that is not shared with eukaryotic type IIA topos.[25,26] The GyrA CTD is a compact circular domain that can bend short DNA segments up to 180° and can constrain positive writhe in larger DNAs.[25,27,28] In the context of the gyrase holoenzyme, the GyrA CTD wraps the DNA flanking a bound G-segment into a local positive-handed crossover, and supplies this DNA *in cis* to the enzyme as a T-segment.[25,27,29] Strand passage inverts this positive crossover into a negative crossover, thereby introducing negative supercoils.[30]

The functional specialization of gyrase prevents the enzyme from effectively catalyzing reactions that involve the capture of a T-segment *in trans*.[16] As a consequence, decatenation and unknotting reactions are left to topo IV in most bacteria.[17,31] Consistent with these primary tasks, topo IV localizes to sites of DNA replication and also interacts directly with the FtsK/Xer chromosome segregation machinery.[32–34] Topo IV efficiently relaxes positive supercoils, such as those formed in front of a DNA replication fork, but is markedly less active on negatively supercoiled DNAs.[35] This selectivity keeps topo IV from relaxing the negative supercoils introduced by gyrase. While the substrate specificity of topo IV is clearly advantageous for bacteria, its selectivity poses a dilemma: how can the enzyme detect and respond to the global topology of a substrate DNA when its small size limits it to sampling only local DNA crossover geometries?

Recent studies have provided valuable insights into how topo IV discriminates between different DNA topologies. Single-molecule experiments using braided DNAs have shown that the enzyme recognizes the local crossing geometry of two DNA duplexes and specifically acts on "left-handed" crossovers, juxtapositions that are found some 25-fold more frequently in positively supercoiled DNA[36,37] (Figure 1(b)). This ratio agrees well with the ~20-fold preference for positive supercoils measured using bulk biochemical methods.[35] In

addition, several experiments have shown that the geometry preference is likely enforced after G-segment binding, suggesting that T-segment recognition is the step in which specificity is imposed.[36–38]

Recently, topo IV has been found to possess a domain in its ParC subunit that is structurally similar to the GyrA CTD and shares the ability to bind and bend DNA *in vitro*.[27,39,40] We have taken a structural and biochemical approach to understand the contribution of this domain (the ParC CTD) to the unique activities of topo IV. Our structural analysis of *Escherichia coli* ParC shows that the CTD is a degenerate form of the GyrA CTD, and that it is positioned relative to the central DNA-binding site so as to interact favorably with incoming T-segments of a certain geometry. Relaxation/decatenation and DNA binding assays using both full-length and CTD-truncated enzymes suggest that the ParC CTD does not influence G-segment binding significantly, but instead acts as a T-segment recruiting element to control substrate specificity. Synthesis of our results with previous findings provides a physical mechanism for the preferential action of topo IV on positively supercoiled and catenated DNAs, and reveals how this enzyme has evolved to act on specific chromosome topologies to support the critical processes of genome replication and segregation in bacteria.

Results

Structure of ParC

To better understand the physical basis for topoisomerase IV function, we undertook a series of structural and mechanistic studies of the ParC subunit and the $ParC_2E_2$ holoenzyme. We first crystallized and solved the structure of the isolated *E. coli* ParC CTD (residues 497–752) to a resolution of 1.7 Å using a combination of single and multi-wavelength anomalous diffraction (SAD/MAD) techniques. This structure was refined to an *R*-factor of 18.4% and a free *R*-factor of 21.6% with good stereochemistry (Table 1). We next designed a construct of *E. coli* ParC (ParC27) optimized for crystallization consisting of amino acid residues 27–742, which represents the full-length subunit minus small protease-sensitive regions (10–26 residues) at its N and C termini (H. Hiasa, personal communication). We crystallized and solved the structure of ParC27 to 3.0 Å resolution by molecular replacement, using the previously solved structure

Table 1. Data collection, refinement and stereochemistry

Data collection	ParC CTD native	ParC CTD SeMet SAD	ParC CTD SeMet MAD peak	ParC CTD SeMet MAD remote	ParC27 native
Resolution (Å)	30–1.70	30–2.0	50–2.0	50–2.0	20–3.0
Wavelength (Å)	1.1271	0.9796	0.9796	1.0199	1.1157
Space group	*P*1	*P*1	*P*1	*P*1	$P2_12_12$
Unit cell dimensions (*a*, *b*, *c*) (Å)	40.91, 50.49, 72.76	41.04, 50.48, 72.87	40.99, 50.53, 72.85	40.99, 50.53, 72.85	257.99, 62.14, 64.00
Unit cell angles (α, β, γ) (deg.)	86.11, 86.91, 70.57	86.37, 86.84 70.78	86.35, 86.89, 70.71	86.35, 86.89, 70.71	90, 90, 90
I/σ (last shell)	22.0 (4.4)	15.3 (3.5)	12.8 (4.7)	14.4 (5.7)	9.5 (2.5)
R_{sym} (last shell) (%)[a]	0.066 (0.257)	0.053 (0.220)	0.043 (0.144)	0.037 (0.120)	0.134 (0.387)
Completeness (last shell) (%)	96.4 (94.1)	96.7 (91.9)	98.0 (96.9)	97.8 (96.8)	89.7 (89.1)
No. of reflections	470,798	273,319	181,740	180,901	217,286
Unique	57,955	72,264	36,477	36,416	19,320
No. of sites	–	16	16	16	–

Refinement	ParC CTD	ParC27
Resolution (Å)	20–1.7	20–3.0
No. of reflections	54,999	18,167
Working	52,062	17,175
Free (% total)	2937 (5%)	992 (5%)
R_{work} (last shell) (%)[b]	18.35 (20.6)	24.04 (35.5)
R_{free} (last shell) (%)[b]	21.55 (23.7)	29.58 (37.2)
Structure and stereochemistry		
No. of atoms	4091	5402
Protein	3711	5367
Water	380	35
r.m.s.d. bond lengths (Å)	0.011	0.007
r.m.s.d. bond angles (deg.)	1.339	1.087

[a] $R_{sym} = \sum\sum_j |I_j - \langle I \rangle| / \sum I_j$, where I_j is the intensity measurement for reflection j and $\langle I \rangle$ is the mean intensity for multiply recorded reflections.

[b] $R_{work,free} = \sum ||F_{obs}| - |F_{calc}|| / |F\text{obs}$, where the working and free *R*-factors are calculated using the working and free reflection sets, respectively. The free reflections were held aside throughout refinement.

of the *E. coli* GyrA core DNA binding/cleavage domains[41] and our structure of the ParC CTD. This structure was refined to a final *R*-factor of 24.0% and a free *R*-factor of 29.6%, and exhibits good stereochemistry (Table 1).

The ParC27 fragment consists of two major regions. The N-terminal region (NTD; residues 28–480) is composed of three domains and adopts a tertiary and quaternary structure highly similar to the equivalent region of GyrA[41] (Figure 2(a)). The first domain, consisting of residues 28–158, contains a helix-turn-helix motif similar to that of the catabolite activator protein (CAP) and contains the active site residues essential for DNA cleavage, Arg119 and Tyr120. The second domain (residues 159–340), termed the "tower," adopts an extended bi-lobed α/β structure that packs against the CAP domain, providing structural support and contributing to the primary DNA binding site. The third domain is a compact α-helical bundle connected by long α-helices to the tower domain and the C-terminal domain. This domain makes up the primary dimer interface of all type IIA topoisomerase structures solved to date.[41–43] In our structure of ParC27, this dimer interface is recapitulated through a crystallographic 2-fold axis (Figure 2(a)).

Three structures of the type IIA topo DNA binding/cleavage domains, one from *E. coli* GyrA and two from *Saccharomyces cerevisiae* topo II, have revealed that these proteins can adopt a range of conformational states. In GyrA, the CAP domains of a dimer contact each other, placing the two active-site tyrosine residues in position to cleave the two

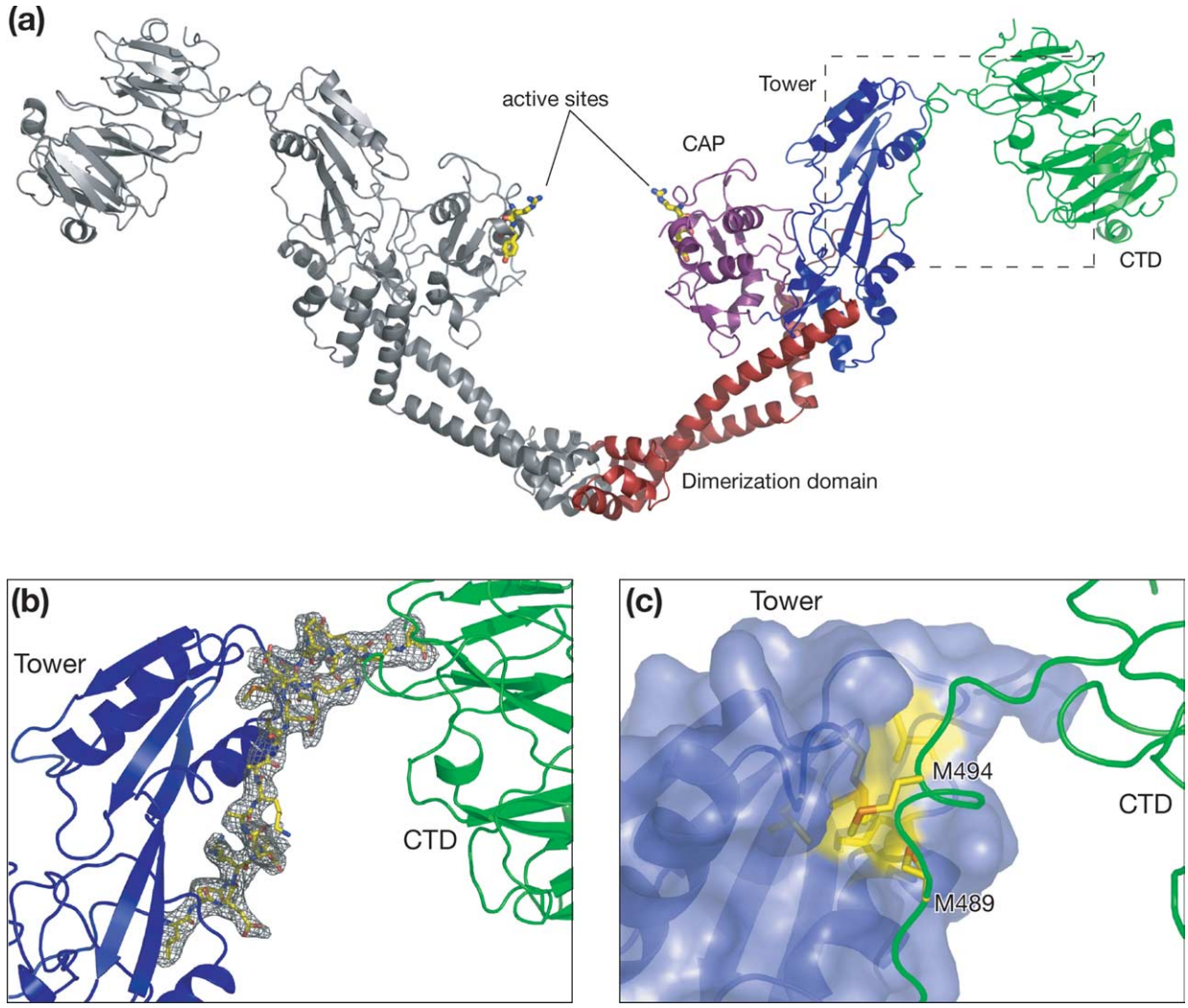

Figure 2. Structure of the full-length ParC subunit. (a) Overall structure of the ParC27 dimer. The CAP domain is colored purple, the tower blue, the dimerization domain and connecting α-helices red, the CTD green, and the active site Arg119 and Tyr120 shown as yellow sticks. The conformation of the dimer is splayed open compared to the structure of the *E. coli* GyrA NTD or *S. cerevisiae* topo II (Figure 3).[41–43] (b) Close-up of the region outlined by the broken box in (a), highlighting the ordered NTD-CTD linker (residues 481–499). Electron density shown is a portion of a simulated-annealing composite all-omit F_o–F_c map, contoured at 2.0σ. (c) View equivalent to (b), showing the hydrophobic "ball joint" formed by two methionine residues on the linker (Met489 and Met494) docking into a hydrophobic pocket on the tower domain (the yellow surface contains residues Leu279, Met281, Val306, Met308, and Val311).

strands of a DNA duplex.[41] By contrast, the CAP domains are seen to move apart from one another in both topo II structures, opening a gap between these elements that separates the two active sites by up to 30 Å.[42,43] Remarkably, ParC27 adopts a more open configuration than seen in any of these structures, separating its active-site tyrosine residues by over 40 Å (Figures 2(a) and 3(a)). This state likely mimics a conformation of the enzyme accessed during strand passage, when the two ends of a cleaved G-segment must be separated to allow the passage of a T-segment. The conformational change from closed to open occurs solely through flexion of the two α-helices that connect the CAP and tower domains to the dimerization domain (Figure 3(b)).

The structure of the ParC DNA binding/cleavage domains also differs from that of GyrA in two loops situated near the active site. A region containing residues 102–124 of ParC, including the active site residues Arg119 and Tyr120, is significantly rearranged in ParC when compared to GyrA (Figure 3(c)). The region also has high *B*-factors, indicating structural flexibility. This difference could reflect functional differences between DNA gyrase and topo IV, but more likely reflects the fact that the CAP domains are separated in our structure of ParC, whereas in GyrA they are dimerized and thus may become more structurally rigid. Residues 55–64 of ParC, which are equivalent to residues 58–67 of GyrA, are also disordered in our structure, probably because the dimer is opened and the adjacent 102–124 loop is rearranged. It should be noted that in our crystals of ParC27, symmetry-related molecules pack against the rearranged 102–124 loop, and probably further contribute to the observed local conformational rearrangements.

The second major region of ParC27, the CTD, comprises residues 500–742. This element is connected by a well-ordered linker (residues 481–499) to the N-terminal region (Figure 2(b)). As anticipated, the CTD adopts a "β-pinwheel" fold, which was first identified in the *Borrelia burgdorferi* GyrA CTD[27] and later observed in the *Bacillus stearothermophilus* ParC CTD[39] and the *E. coli* GyrA CTD[28] (Figure 4). The architecture of the β-pinwheel fold is reminiscent of a β-propeller, but the Greek key-like topology of its four-stranded β-sheet "blades" is distinct from the antiparallel hairpin sheets found in β-propellers.[27] One hallmark of the β-pinwheel fold is that the outer-most strand of each blade associates with the inner strands from the previous blade, creating an interlocking structure that holds the blades together (Figure 4(a) and (d)).

Two structures of the GyrA CTD, from *B. burgdorferi* and *E. coli*, have shown that this domain is made up of six blades that pack into a circular structure.[27,28] Interestingly, one difference between these structures is that the "GyrA box," the motif that holds the *B. burgdorferi* GyrA CTD in a closed ring by locking blade 1 onto blade 6, is disordered in the *E. coli* domain, allowing this CTD to adopt a spiral shape.[28] A distinguishing feature of all ParC CTDs is that they universally lack the GyrA box motif (Figure 4(b) and (d)).[40] As a consequence, the *B. stearothermophilus* ParC CTD was also observed to adopt an open, spiral conformation highly similar to that of the *E. coli* GyrA CTD.[39] Upon solving the structure of the *E. coli* ParC CTD, we observe that it too adopts an open C-shaped structure, although the pitch of the spiral in this domain is markedly reduced compared to the other spiral-shaped CTD structures, and it also lacks one entire blade (Figure 4; Supplementary Data, Figure S1). In the GyrA CTD, the spiral shape of the *E. coli* domain is thought to impart a directional bias to the domain's DNA wrapping ability to enhance supercoiling activity.[28] It is as yet unknown how this phenomenon might affect the properties of topoisomerase IV. Despite these structural differences, all GyrA and ParC CTDs share a key feature: a positively charged outer rim thought to comprise a DNA binding/bending surface[27,39] (Figure 4(c)).

During the catalytic cycle of gyrase, the GyrA CTD is thought to cycle between two different locations: an "upper" position where the CTD lies near the tower domain and interacts with the DNA flanking a G-segment,[26,44] and a "lower" position near the connector α-helices that could represent either a pre-DNA-binding or post-strand passage state.[45] In our structure of ParC27, the CTD resides at the very top of the tower domain in a location analogous to the upper position observed for the GyrA CTD (Figure 2(a)). The linker attaching the N and C-terminal domains in ParC27 is well-ordered in refined $2F_o - F_c$ and simulated annealing omit electron density maps (Figure 2(b)), and it wraps around the tower domain for most of its length. Four residues between the NTD and the CTD (residues 496–499) are ordered in the structure, but are entirely solvent-exposed and do not pack against either domain. Two hydrophobic residues (Met489 and Met494) just upstream of this accessible segment are conserved in ParC orthologs and dock into a hydrophobic patch on the NTD (Figure 2(c)). This type of hydrophobic "ball joint," especially involving flexible methionine residues, has been proposed to allow a degree of plasticity in protein–protein interfaces while maintaining a tight association between the interacting partners.[46,47] Together, these features likely permit the CTD to rotate with respect to the N-terminal region, but constrain it in a location analogous to the upper position of the GyrA CTD.

Supercoil relaxation and decatenation by topo IV +/− ParC CTD

To determine the role of the ParC CTD in supercoil relaxation and decatenation, we reconstituted topo IV $ParC_2E_2$ heterotetramers using either wild-type or CTD-truncated (residues 2–482) ParC. We confirmed holoenzyme formation using analytical gel filtration (see Materials and Methods), and tested the activity of the reconstituted enzymes on a number of different substrates. Comparison of

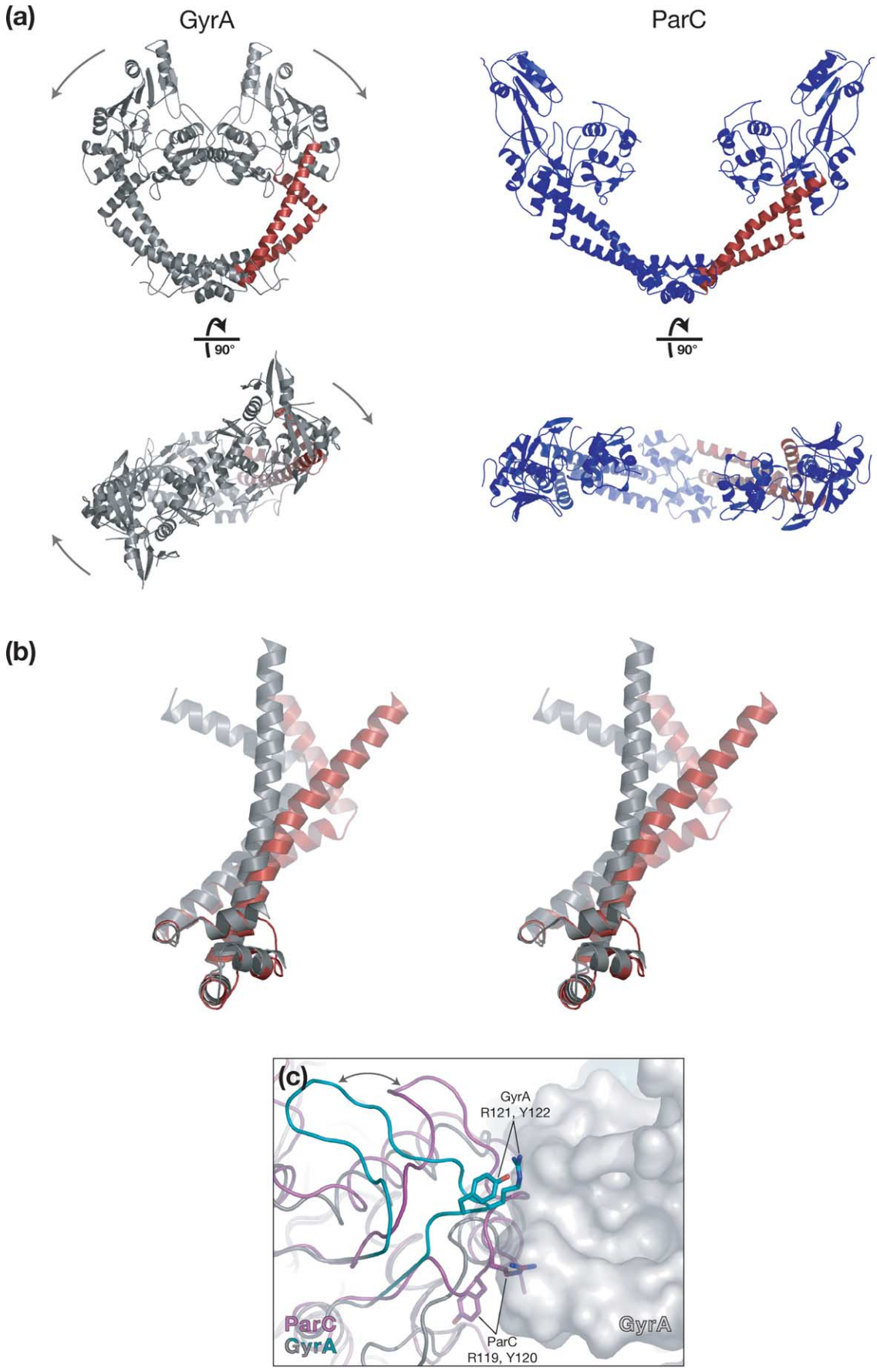

Figure 3 (*legend on next page*)

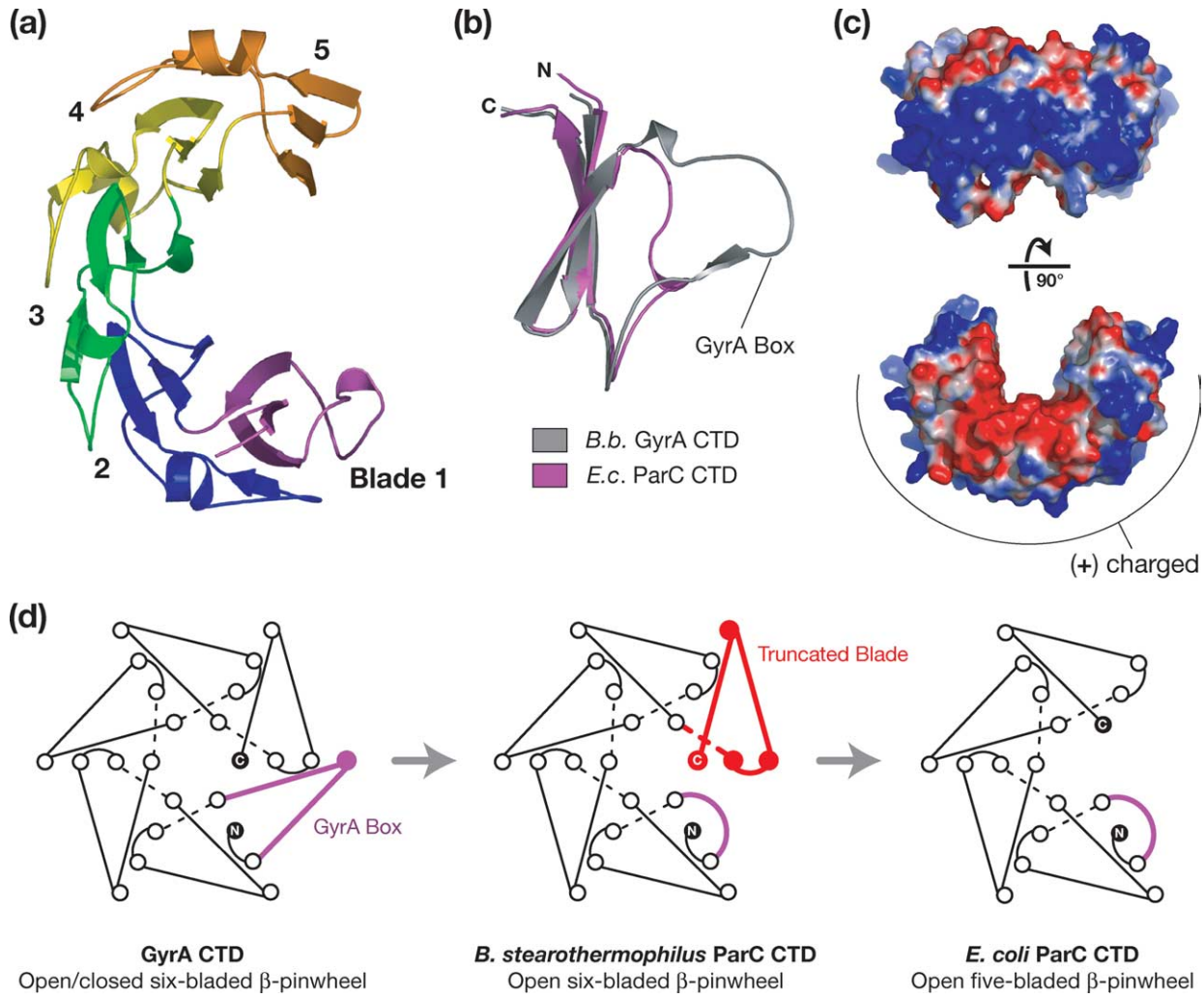

Figure 4. Structure of the ParC CTD. (a) Top view of the *E. coli* ParC C-terminal domain. Blades 1–5 are labeled and colored purple, blue, green, yellow, and orange, respectively. (b) Overlay of blade 1 of the *E. coli* ParC CTD (purple) with that of the *B. burgdorferi* GyrA CTD[27] (gray), showing that the GyrA box motif is deleted in ParC. (c) Side and top views of the electrostatic surface of the ParC CTD, showing the curved, positively charged outer surface that likely comprises its DNA binding surface.[27] (d) Structural relationships between the different bacterial type IIA topo CTDs. CTDs with an intact GyrA box motif can adopt open or closed conformations, potentially depending on the sequence of the GyrA box (Supplementary Data, Figure S2). Truncation of the GyrA box (purple) from the six-bladed GyrA CTD[27,28] (left) gives rise to the open six-bladed CTD found in some ParC orthologs[39] (middle). The further loss of one full blade (shown here as blade six, in red) gives rise to the open five-bladed ParC CTD of *E. coli* and other Proteobacteria (right) (also see Figure 8).

the activities of wild-type and CTD-truncated topo IV on negatively supercoiled DNA revealed a ~10-fold reduction in relaxation activity upon the removal of the ParC CTD (Figure 5(a)).

Since topo IV has been shown to relax positive supercoils ~20 times more efficiently than negative supercoils,[35] we next tested the effect of the ParC CTD truncation on the relaxation of positively supercoiled DNA (Figure 5(b)). We observe that the wild-type enzyme is indeed much more active (~15-fold) on the positively supercoiled substrate when compared to its activity on negative supercoils. Interestingly, this robust relaxation activity drops about 100-fold upon ablation of the ParC

Figure 3. Comparison of GyrA and ParC NTD conformations. (a) The N-terminal regions of GyrA[41] (gray) and ParC (blue) are presented side-by-side. Shown in red are a pair of α-helices that connect the dimerization domain to the CAP and tower domains. Top-down views show that a twisting motion accompanies the separation of the CAP domains (arrows). (b) Stereo view of an overlay of one dimerization domain from GyrA (gray) and ParC (red), showing the flexion of the connector helices that leads to the global conformational differences observed between the two structures. Not shown in this panel is an insertion in the dimerization domain (residues 413–451) specific to GyrA. (c) Top-down view of the active site of ParC (purple) overlaid with that of GyrA (gray and cyan, dimer mate in gray surface). The reconfigured loop in the CAP domain (residues 102–124 of ParC) is shown with active-site arginine and tyrosine residues (labeled) in stick representation.

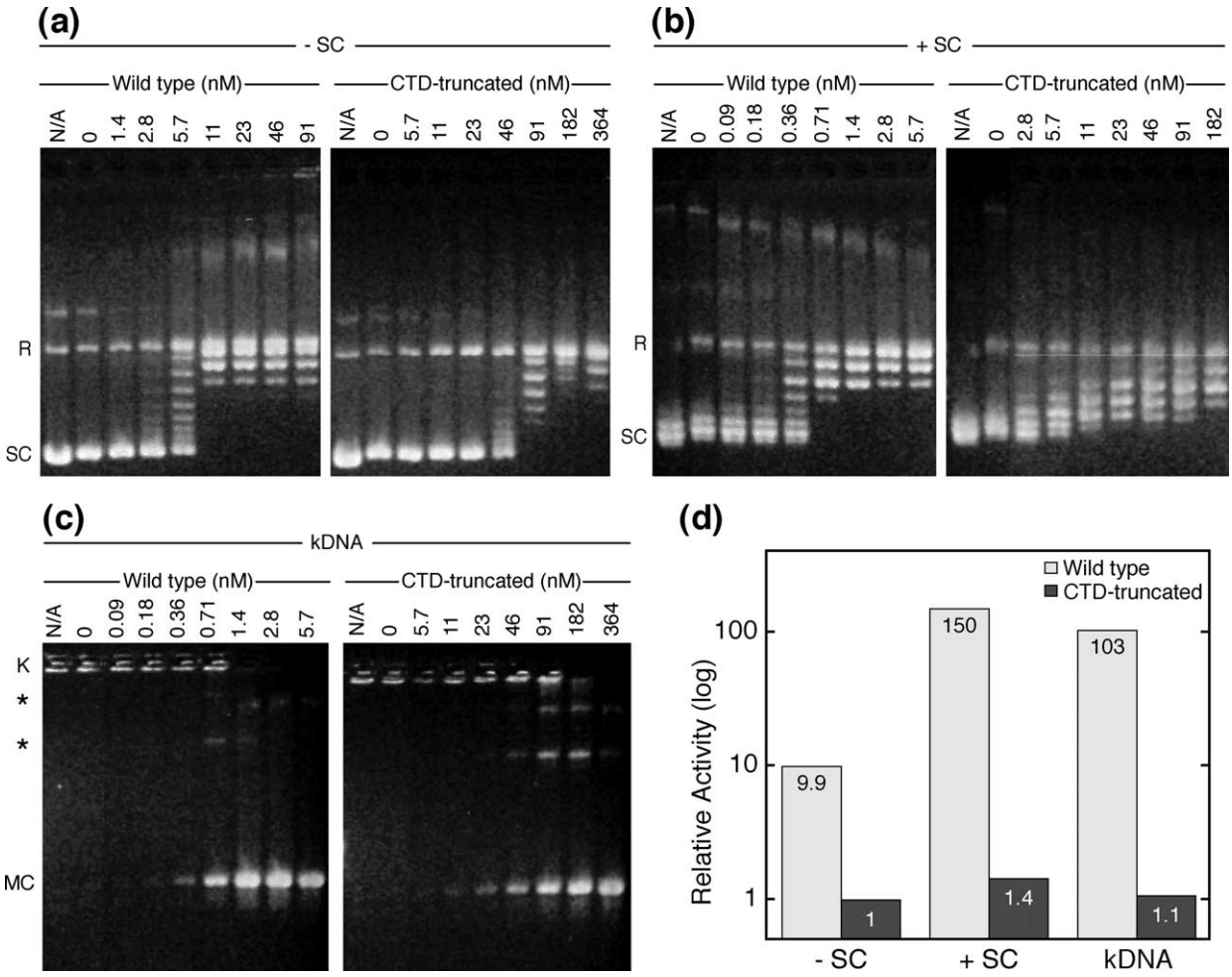

Figure 5. DNA relaxation and decatenation by wild-type and CTD-truncated topo IV. Reconstituted wild-type or CTD-truncated topo IV was incubated at various concentrations (indicated above each lane, in nM topo IV) with negatively supercoiled plasmid (a), positively supercoiled plasmid (b), or kDNA (c). The positions of negatively and positively supercoiled DNA are indicated on the left-hand side of each panel by SC, and the distribution of relaxed topoisomers is indicated by R. In the decatenation assay (c), the unreacted kDNA network (K, left side) does not enter the gel, and remains in the wells. Fully decatenated mini-circles are indicated by MC, and incompletely decatenated products are indicated with asterisks (*). (d) Quantification of enzyme activities from (a)–(c). The specific activities of the two enzymes on each substrate were quantified (see Materials and Methods), normalized to that of CTD-truncated topo IV on negatively supercoiled DNA, and plotted on a log scale.

CTD. Comparison of the activity of the CTD-truncated enzyme on positively and negatively supercoiled DNAs reveals that without the ParC CTD, the enzyme relaxes supercoils of either polarity with similar efficiencies (Figure 5(d)).

Topo IV's decatenation activity is also dramatically affected by removal of the ParC CTD. Figure 5(c) shows the activity of wild-type and CTD-truncated topo IV on kinetoplast DNA, a system of relaxed, highly catenated 2.5 kb DNA minicircles classically used in decatenation assays.[48–50] The kinetoplast DNA network is too large to enter the gel, so unreacted substrate remains in the wells and decatenated product appears as a single band. As with positively supercoiled DNA, truncation of the ParC CTD results in a ~100-fold reduction in decatenation activity by topo IV.

Overall, these data show that while wild-type topo IV is a robust decatenase and relaxes positive supercoils much more efficiently than negative supercoils, removal of the ParC CTD reduces the enzyme's activity on all substrates to a similar "baseline" level. Strikingly, the CTD enforces substrate specificity by activating the enzyme up to 100-fold on its preferred substrates (positively supercoiled and catenated DNAs), while activating the enzyme to a lesser degree on negatively supercoiled DNA (Figure 5(d)). Time-course experiments performed with reconstituted enzymes held at a fixed concentration showed similar results for all assays (data not shown). Taken together, these data indicate that the ParC CTD is an important structural determinant of topo IV's specificity for catenanes and positively supercoiled DNA.

DNA binding by topo IV +/− ParC CTD

To ensure that the reduction in topo IV activity

arising from removal of the ParC CTD did not result simply from a loss in DNA binding affinity, we next performed DNA binding assays with full-length and CTD-truncated topo IV. As shown in Figure 6, the full-length and CTD-truncated enzymes bind DNA with very similar affinities in filter-binding experiments (K_d = 119 (∓8) nM for wild-type, 79 (∓22) nM for CTD-truncated). This finding shows that removal of the ParC CTD does not exert its effects on activity simply by weakening the enzyme's ability to associate with DNA. It should be noted that while the DNA-binding affinities we observe are lower than those reported for wild-type topo IV,[36,38] this difference likely arises from the use of chloride instead of glutamate as the predominant anion in our assays. This change was necessary to overcome modest aggregation of the CTD-truncated enzyme at low ionic strength in the presence of glutamate (data not shown).

Interestingly, the fractional saturation of the DNA-binding curve for CTD-truncated topo IV is reproducibly about half that of the wild-type enzyme (maximum fraction DNA bound = 0.52 ∓ 0.01 for wild-type, 0.26 ∓ 0.02 for CTD-truncated) (Figure 6). A concern with these data is that neither protein bound DNA at levels approaching full saturation. This again may be due to the use of chloride instead of glutamate in our assays, which could decrease the half-life of the protein–DNA interaction and allow DNA to be washed off the membrane more readily. As such, it is possible that the lower fractional saturation achieved with CTD-truncated topo IV is due to an increased dissociation rate compared to the wild-type enzyme. Alternatively, since the CTD-truncated enzyme consistently binds half as much DNA as the wild-type enzyme, it may be that wild-type topo IV is able to bind two DNA segments, while the CTD-truncated enzyme has lost the ability to bind one of these segments. Since both the wild-type and CTD-truncated topo IV constructs retain the primary G-segment binding site, the simplest interpretation of these results is that the ParC CTD makes up a T-segment binding site, and that this site is lost upon CTD truncation. This interpretation is supported by our relaxation and decatenation data, which suggests that the ParC CTD is involved in T-segment selection. In addition, our results agree with footprinting data showing that topo IV protects a region of the G-segment corresponding only to the primary DNA binding site, implying that no other elements of the enzyme are involved in G-segment binding.[38]

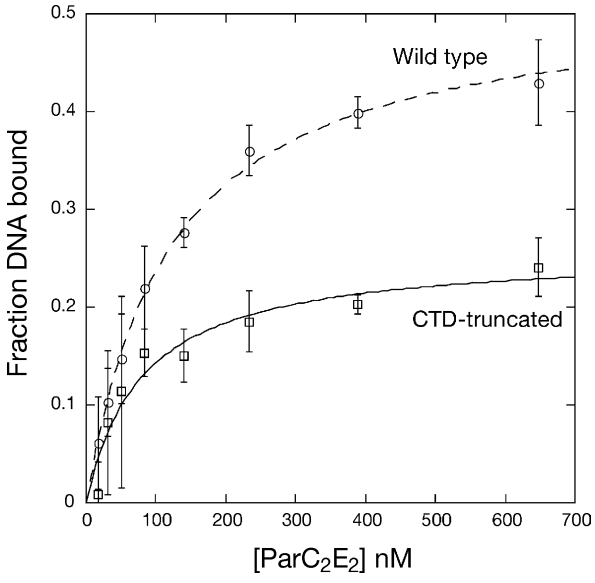

Figure 6. DNA binding by wild-type and CTD-truncated topo IV. Linearized, ^{32}P-labeled plasmid (0.5 nM) was incubated with varying amounts of reconstituted wild-type (circles, broken line) or CTD-truncated topo IV (squares, continuous line). The fraction of DNA retained by the nitrocellulose filter is reported as the fraction bound to protein. Data points represent averages of triplicate readings, error bars represent standard deviations, and lines indicate the fit to an independent binding sites model (see Materials and Methods).

Discussion

The ParC CTD is a DNA geometry sensor

The data presented here allow us to explain how structural differences between two paralogous type IIA topoisomerases in *E. coli* lead to distinct functional profiles. In gyrase, it is thought that the GyrA CTD binds 40–50 base-pairs of DNA flanking a bound G-segment and imposes a "U-turn" on the DNA so that it wraps around the enzyme to be used as a T-segment *in cis*[25,27,28,51,52] (Figure 7(a)). This juxtaposition creates a positive crossover that is converted into a negative crossover upon strand passage, resulting in the introduction of negative supercoils into substrate DNA. Interestingly, the GyrA CTD appears to be only loosely tethered to the N-terminal region, and may adopt at least two positional states: an "upper" orientation for wrapping DNA prior to strand passage,[44] and a "lower" position that may represent a resting or post-strand passage state.[45] It has been proposed that the GyrA CTD may be able to cycle between these conformations during the strand passage cycle, and that this motion could be important for shuttling a T-segment through the enzyme.[45]

While topo IV has been shown to act specifically on positive crossovers and catenated DNAs, how the enzyme discriminates between different substrates is not understood. Recent experiments have shown that the substrate specificity of topo IV derives from a preference for binding incoming T-segments of a specific geometry, so-called "left-handed crossovers," that occur more often in positively supercoiled DNA[36,37] (Figure 1(b)). DNA footprinting studies on gyrase and topo IV have indicated that despite their close homology, topo IV binds only a short (~30 bp) region of G-segment DNA,[38] in contrast to the extended 120–150 bp footprint of gyrase.[51,53,54] Topo IV binds

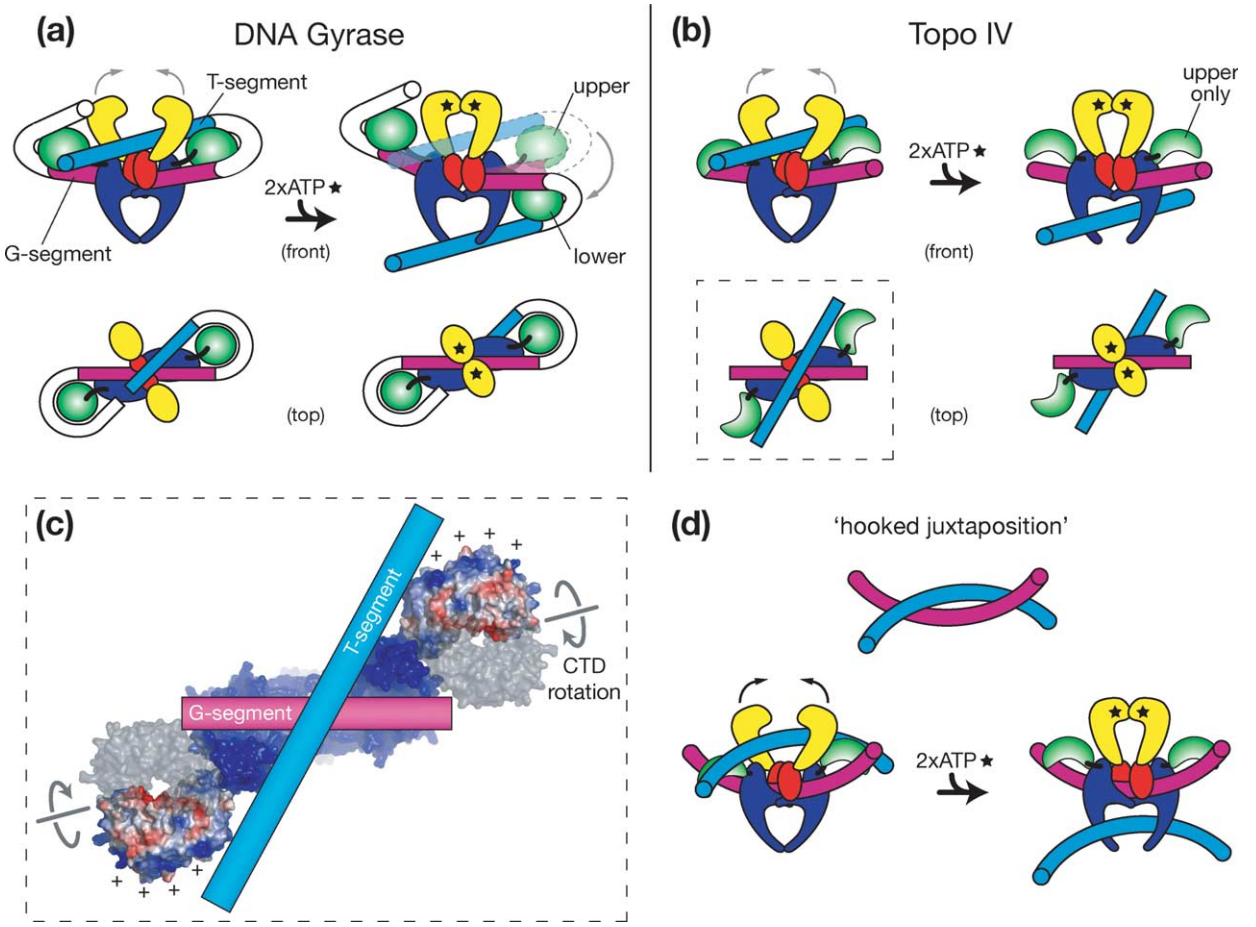

Figure 7. Model for the substrate specificity of bacterial type IIA topos. (a) Model for the contribution of the GyrA CTD to the reactions of DNA gyrase.[27,45] Domains of the enzyme are colored yellow (ATPase), red/blue (DNA binding/cleavage), and green (CTD). T and G-segments are labeled and colored cyan and magenta, respectively. The CTD may transition between an upper and a lower state upon strand passage. (b) Model for the contribution of the ParC CTD to the reactions of topo IV. The CTDs are anchored near the top of the N-terminal region, where they may aid the binding of a T-segment and favor interactions with crossovers of the correct left-handed geometry (see Figure 1(b)). (c) Top-down view of ParC27 showing how the CTDs might rotate from their location in the crystal structure (transparent gray surface) to a location (electrostatic surface) where their positively charged outer surface (shown in blue) may interact with a T-segment that forms a left-handed DNA crossover with a bound G-segment. The rotation was modeled about Ser496, one of the four unconstrained residues linking the N and C-terminal domains. (d) Model for topo IV acting on hooked juxtapositions. Two DNA segments curved toward each other may form an attractive substrate for topo IV; in this scheme, the ParC CTDs could recognize and/or reinforce the bending of a T-segment.

supercoiled DNA more tightly than linear, but does not distinguish positively from negatively supercoiled DNA at this step, indicating that G-segment binding is not sufficient to distinguish crossover geometry.[36–38] Together, these results have suggested that the substrate specificity of topo IV may arise from the capture of incoming T-segments with particular crossing angles.[39]

Our current studies strongly support this model. Structural and biochemical data demonstrate that the ParC CTD is the major determinant for substrate selection by topo IV, and that this behavior likely arises from direct interactions with the T-segment. In the absence of the ParC CTD, topo IV acts on different substrates at a single low "baseline" level (Figure 5). With the CTD, however, the activity of topo IV is enhanced on all substrates, particularly on positively supercoiled and catenated DNAs. This behavior can be explained by a scheme in which the ParC CTD not only helps recruit T-segments *in trans*, but also selects for crossover geometries common in positively supercoiled or catenated substrates (Figure 7(b) and (d)).

Our crystallographic studies provide a physical framework with which to understand this behavior. The structure of ParC27 shows that the ParC CTD is anchored to the top of the tower domain, but is probably free to rotate about its attachment point. A simple rotation of the ParC CTD by 90–180° from the position observed in the crystal readily orients this domain where it may associate with T-segments that enter the enzyme in the left-handed configuration characteristic of positively supercoiled DNA (Figure 7(c)).

This physical model also may account for the robust decatenation activity of topo IV. Although

most catenated DNAs should have no bias in crossover angle, a recent computational study by Buck *et al.* proposed that type IIA topoisomerases may specifically recognize catenated and knotted DNA crossings by virtue of the two DNA segments curving toward each other in a "hooked" juxtaposition.[55] The authors propose that the ability of type IIA topoisomerases to bend a bound G-segment "upward" toward an incoming T-segment allows them to specifically recognize crossovers in a hooked geometry. With respect to topo IV, hooked geometries may be a general feature of DNA crossovers that this enzyme has evolved to recognize. For example, the two DNA duplexes in plectonemic supercoils curve toward each other, and a similar geometry is likely found in the positive-handed precatenanes that occur behind a DNA replication fork[1] (Figure 1(a)). The relative positioning of the N and C-terminal domains of ParC, together with the CTD's ability to bend DNA,[27] could allow the enzyme to specifically bind T-segments bent toward the bound G-segment (Figure 7(d)). Thus, topo IV may recognize both DNA segments of a hooked juxtaposition, in contrast to canonical type II topos, which specifically recognize only one. Consistent with this possibility, topo IV is significantly more effective at recognizing and resolving knotted and catenated DNA crossovers than eukaryotic type IIA topos, which lack a homologous C-terminal domain.[56,57]

Given the structural similarity and evolutionary relatedness between topo IV and DNA gyrase, it might be expected that the actions of the GyrA and ParC CTDs parallel one another to a certain extent. Indeed, our models invoke highly similar roles for these two domains, particularly when considering the different activities of these enzymes, and the fact that the DNA crossover imposed by the GyrA CTD likely adopts a geometry very much like that recognized by the ParC CTD (Figure 7(a) and (b)). It should be noted, however, that instead of imposing proper crossover geometry as per GyrA, ParC can only recognize it. In addition, the ParC CTD does not bind or bend DNA as effectively as its counterpart in gyrase,[27] and thus may not be able to stabilize the DNA wrap required to negatively supercoil DNA. Together, the two enzymes represent an elegant example of how modest structural change can significantly impact enzymatic and biological function.

Evolution of bacterial type IIA topoisomerases

Of the two paralogous type IIA topoisomerases found in *E. coli*, topo IV has sometimes been considered to possess the more "canonical" enzyme activity and cellular function. By contrast, DNA gyrase has usually been thought of as a specialized enzyme evolved primarily to supercoil DNA. Recent studies, however, have clearly shown that topo IV is as functionally specialized as DNA gyrase. This information, along with emerging phylogenetic and structural data on both DNA gyrase and topo IV, has begun to paint a new picture of how bacterial type IIA topoisomerases likely evolved.

With the *E. coli* ParC CTD structure presented here, there now exist four distinct views of β-pinwheel domains. These structures, along with phylogenetic analyses and secondary structure prediction (Figure 8), indicate that all GyrA CTDs possess six full blades and an intact GyrA box sequence, which may or may not close the β-pinwheel into a circular structure (Supplementary Data, Figure S2), and likely also plays a role in DNA binding by the domain.[27,28] The evolution of topo IV from this framework seems to have coincided with the progressive loss or alteration of structural features from this core domain, concomitant with functional modification of the enzyme. The first step in this sequence was likely the truncation of the GyrA box as observed in the *B. stearothermophilus* ParC CTD structure,[39] which may have compromised the domain's DNA wrapping function to some extent, in addition to enforcing the open spiral conformation. Functionally, this change likely abolished the supercoiling activity of the enzyme and allowed it to select for the binding and passage of DNA duplexes *in trans*. The open six-bladed ParC CTD architecture is found throughout the Firmicutes, encompassing the Bacilli and Mollicutes, and also in the Actinobacteria (Figure 8). In addition to the loss of the GyrA box, the ParC CTDs of the Proteobacteria are missing one entire blade, resulting in the five-bladed, open β-pinwheel typified by the ParC CTD of *E. coli*. Still other groups of bacteria appear to have gained more blades (Clostridia), lost most or all of the ParC CTD (the Spirochetes and Chlamydiales), or lack topo IV entirely (the Bacteroidetes/Chlorobi group, ε-Proteobacteria, and most Mycobacteria)[27] (Figure 8). The deepest branches, possibly representing ancestral enzymes, contain CTDs whose lineage is somewhat ambiguous, but may be more GyrA-like. These incremental changes within the ParC family, together with wider distribution and higher conservation of gyrase than topo IV, indicate that ParC CTDs are degenerate forms of the GyrA CTD and that modern bacterial type IIA topoisomerases likely evolved from a gyrase-like enzyme. Interestingly, these findings echo the conclusions of an earlier study of bacterial type IIA topos, which found similar relationships by comparing the primary DNA binding regions in the NTDs of GyrA and ParC proteins.[22]

The surprising structural variety in the β-pinwheel domains of different bacterial type IIA topos, together with the significant functional effects that appear to result from these structural changes, implies that there may exist a wide range of enzymes with activity profiles distinct from those of *E. coli* gyrase and topo IV. For example, there may be instances where the division of labor between the two enzymes is distinct from those found in *E. coli*, and some bacteria likely possess a single type IIA topoisomerase able to perform all functions

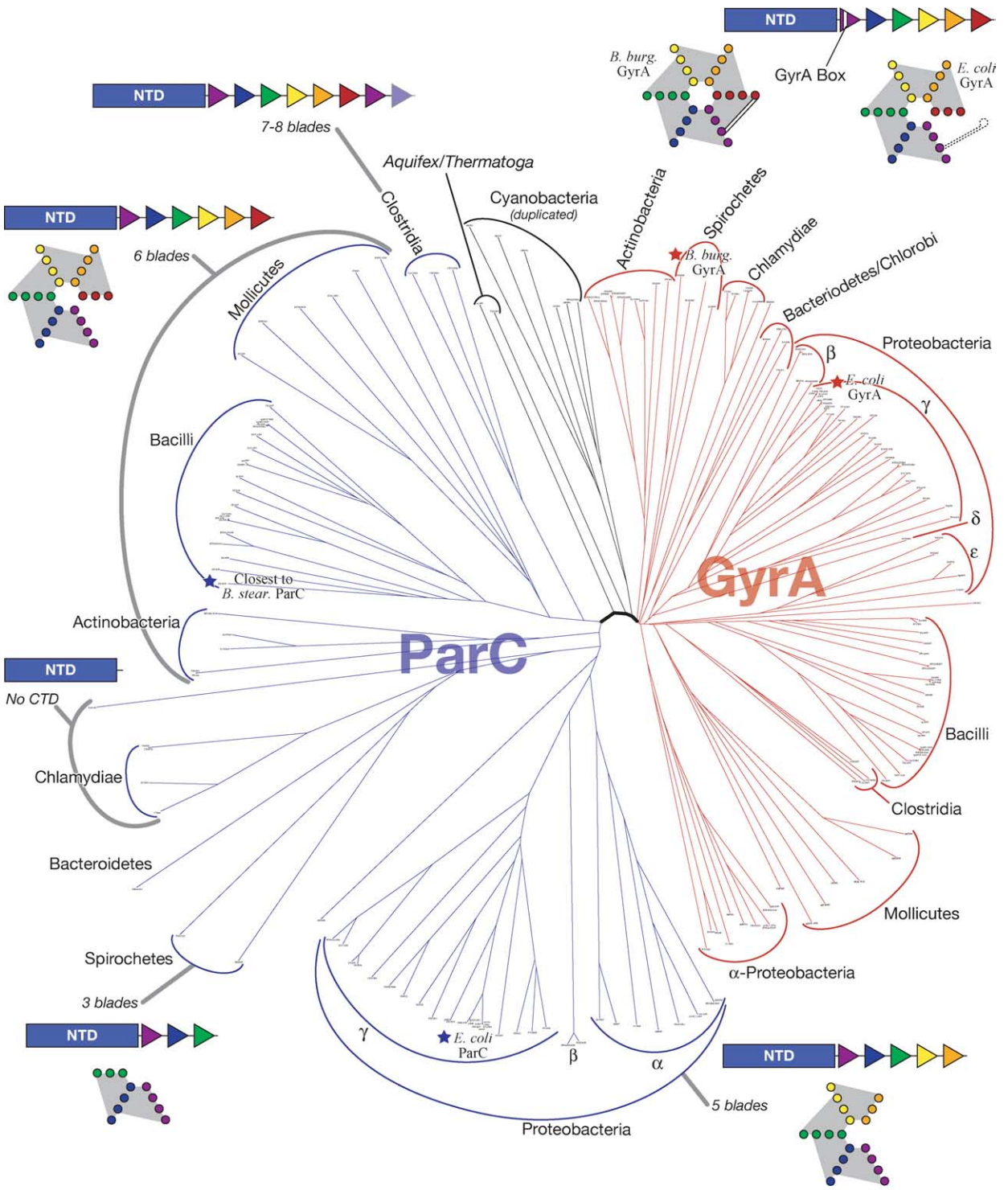

Figure 8. Phylogenetic tree of full-length GyrA and ParC sequences. ParC sequences are shown in blue, GyrA sequences in red, and more ambiguous genes from *Aquifex aeolicus* and *Thermatoga maritima*, as well as from Cyanobacteria (which each possess two very similar GyrA proteins, one with a truncated GyrA box) are shown in black. Note that the branch lengths are longer overall for ParC *versus* GyrA, and that different subfamilies of ParC proteins are better defined by deep branches. Families of GyrA/ParC proteins are noted at the perimeter, along with representations of the probable CTD architecture in each family. The locations of the four CTD structures are noted with stars (*B. stearothermophilus* ParC was not included in the alignment, since the full-length ParC sequence corresponding to the structure is not available; however, its closest sequence relative (*B. subtilis*) is noted[27,39]). It is currently unknown how various GyrA C-terminal domains partition between the closed, *B. burgdorferi*-like and the open, *E. coli*-like architechtures, but it is likely that the open form is more prevalent (see Figure S2). CTD architectures in those families for which structures are not available were inferred from inspection of the sequences and PSIPRED secondary structure predictions of subfamily sequence alignments.[80] Protein sequences used for the alignment can be found in Supplementary Data, Table S1.

attributed to gyrase and topo IV. In support of these ideas, a recent study found that DNA gyrase from *Mycobacterium smegmatis* possesses significant decatenase activity in addition to its supercoiling capability.[58] This behavior may reflect the need for a minimal level of decatenation function in the Mycobacteria, a group that largely lacks topo IV. Interestingly, the recently sequenced genome of *M. smegmatis* revealed that this organism, the only "rapid growing" mycobacterium sequenced to date,[59] is also the only sequenced mycobacterium to contain a topo IV homolog (The Institute for Genome Research†). Thus, it may be that growth rate is one important factor determining an organism's topoisomerase needs: the faster a cell divides, the more it may require a dedicated decatenating enzyme (topo IV) to avoid chromosome partitioning defects.

Conclusion

It is becoming evident that bacterial type IIA topoisomerases are highly specialized to satisfy specific cellular needs. The GyrA and ParC C-terminal domains have emerged as important elements that help define these enzymes' unique activity profiles, and minor alterations to CTD structure or positioning can generate profound functional changes. This work shows how the *E. coli* ParC CTD helps control the substrate specificity of topo IV, and reveals that this mechanism exhibits significant parallels and contrasts with that of the paralogous DNA gyrase. Our findings suggest that the classic functional definitions of DNA gyrase and topo IV may be too restrictive, and that there may be a continuum of functions among bacterial type IIA topoisomerases. Further study of these enzymes from a range of bacteria will illuminate how type IIA topoisomerases are fine-tuned to meet specific needs for regulating chromosome superstructure during DNA replication, repair, and segregation.

Materials and Methods

Cloning and protein purification

Constructs containing residues 497–752 (ParC CTD) or 27–742 (ParC27) of *E. coli* ParC were amplified from genomic DNA (ATCC) and cloned into pET28b behind an N-terminal, tobacco etch virus (TEV) protease-cleavable His_6 tag. The full-length *E. coli parE* and *parC* genes, as well as a CTD-truncated *parC* (ParC NTD) (residues 2–482) were also cloned into the same vector.

Proteins were overexpressed in *E. coli* BL21-CodonPlus(DE3)-RIL cells (Stratagene) by inducing with 0.5 mM isopropyl-β-D-thiogalactopyranoside (IPTG) at $A_{600}=0.3$ for four hours at 37 °C (six hours at 30 °C for ParC NTD). Most cell cultures were harvested by centrifugation, resuspended in buffer A (20 mM Hepes (pH 7.5), 10% (v/v) glycerol, 2 mM β-mercaptoethanol) plus 800 mM NaCl, 10 mM imidazole, 50 μg/ml of lysozyme, and protease inhibitors, and frozen drop-wise into liquid nitrogen. Cells expressing the ParC NTD were harvested and resuspended in buffer B (50 mM Tris–HCl (pH 7.5), 20% glycerol, 2 mM β-mercaptoethanol) plus 800 mM NaCl, 10 mM imidazole, 50 μg/ml of lysozyme, and protease inhibitors, and frozen.

For protein purification, cells were sonicated and centrifuged, and the clarified lysate passed over a Ni^{2+}-affinity column (Amersham). Peak fractions were pooled, concentrated and incubated overnight at 4 °C with His_6-tagged TEV protease[60] using a ratio of 1:50–1:10 (w/w) TEV protease/protein. This mixture was again passed over a Ni^{2+}-affinity column to remove uncleaved protein, the cleaved His_6-tag, and TEV protease. Proteins were then run over S200 or S300 gel filtration columns (Amersham Biosciences), except for the ParC NTD, which was further purified over a HiTrap Q ion-exchange column (Amersham Biosciences). Proteins used for crystallography were concentrated by ultrafiltration and kept at 4 °C. Proteins used for biochemical assays were flash-frozen in aliquots and stored at −80 °C. Purification of selenomethionine-labeled ParC CTD, prepared by the method described by Van Duyne *et al.*,[61] was performed as for native protein, with the addition of 1 mM Tris(2-carboxyethyl)phosphine (TCEP) (Fluka) in the gel-filtration step and thereafter.

To confirm that the two ParC constructs formed heterotetramers with similar efficiency, equimolar amounts of ParC and ParE subunits were mixed, incubated 30 minutes on ice, and passed over an analytical gel filtration column (Superdex-200 HR 10/30; Amersham Biosciences) (data not shown).

Crystallization, data collection, and structure solution

For crystallization of the *E. coli* ParC CTD, purified protein (15–25 mg/ml) was dialyzed overnight at 4 °C against 20 mM Hepes (pH 7.5) and 100 mM NaCl (plus 0.5 mM TCEP for selenomethionine-labeled protein). Crystals were grown at 19 °C or 4 °C in hanging drop format by mixing 1 μl of protein with 1 μl of well solution (100 mM sodium acetate (pH 4.5), 50 mM ammonium acetate, and 20% (w/v) polyethylene glycol (PEG) 4000). For harvesting, a cryoprotectant solution containing well solution plus 25% ethylene glycol was added directly to the drop, and the crystals were immediately looped and flash-frozen in liquid nitrogen.

Crystals of ParC27 were grown in hanging drop format by mixing 1 μl of purified protein (20 mg/ml) in buffer A plus 200 mM NaCl with 1 μl well solution (20 mM Hepes (pH 7.5), 10% glycerol, 100 mM NaCl, 4% PEG 6000, and 8% (v/v) 1,3-butanediol). For harvesting, a cryoprotectant solution containing well solution plus 20% PEG 400 was added directly to the drop, and the crystals were immediately looped and flash-frozen.

All datasets were collected on Beamline 8.3.1 at the Advanced Light Source at Lawrence Berkeley National Laboratory.[62] Data were indexed and reduced with HKL2000[63] or ELVES[64] using MOSFLM.[65]

For the *E. coli* ParC CTD, phasing was performed using single and multi-wavelength anomalous diffraction (SAD/MAD) methods with selenomethione-substituted crystals. Selenium sites were first located using SOLVE[66] from a single-wavelength dataset (SeMet SAD; Table 1). These sites were supplied to MLPHARE[67] along with a

† www.tigr.org

multi-wavelength dataset (SeMet MAD Peak and Remote; Table 1) for phase calculation and refinement, and density modification was performed using DM[67] to produce initial electron density maps. A preliminary model of the ParC CTD was built with RESOLVE,[66] and manual rebuilding was performed with O.[68] Refinement was carried out using a Refmac/ARP procedure to automatically place ordered water molecules,[69] followed by TLS refinement in Refmac5.[70] The final model consists of two chains of amino acid residues 497–742 of the ParC CTD; residue 694 of chain A and residues 743–752 of both chains are missing from the model. A total of 94.6% of non-glycine residues are in the most favored regions of Ramachandran space, and none are in disallowed regions.

For ParC27, molecular replacement was performed at 3.0 Å resolution using PHASER,[71] searching with poly-serine models of the ParC CTD and the CAP and tower domains (residues 30–362) of *E. coli* DNA gyrase A.[41] The remaining domains of *E. coli* GyrA (residues 363–522) were placed manually into initial maps produced by PHASER. Solvent flattening was performed with DM[67] and prime and switch phasing was performed with RESOLVE[66] to produce electron density maps suitable for manual rebuilding. Multiple rounds of simulated annealing refinement in CNS[72] and manual rebuilding reduced the free *R*-factor to ~34%. TLS refinement in Refmac5 and manual placement of ordered water molecules yielded a final *R*-factor of 24.0% and a free *R*-factor of 29.6% (Table 1). The final model consists of residues 28–740 of ParC, with disordered loop residues 55–64, 516–530, and 565–567 missing from the model. A total of 86.5% of non-glycine residues are in the most favored regions of Ramachandran space, and no residues are in disallowed regions. Electrostatic surfaces were calculated with APBS.[73] All molecular Figures were produced with PyMOL.[74]

DNA relaxation/decatenation assays

Plasmid pSG483, a 3 kb derivative of pBluescript II SK (Stratagene), was used for supercoiled DNA substrates. Negatively supercoiled plasmid was purified from *E. coli* XL1 Blue cells using CsCl gradients. Positively supercoiled DNA was made using *A. fulgidus* reverse gyrase.[75] Kinetoplast DNA (kDNA) from *Crithidia fasciculata* was purchased from Topogen. DNA relaxation or decatenation assays (20 μl) were performed in a buffer containing 50 mM Tris-HCl (pH 7.8), 6 mM $MgCl_2$, 10 mM DTT, 1 mM ATP, 20 mM KCl, 1 mM spermidine, 100 μg/ml bovine serum albumen (BSA), with 300 ng supercoiled DNA or kDNA. Varying amounts of reconstituted wild-type or CTD-truncated topo IV were added to reaction mixtures, and reactions were allowed to proceed for 30 minutes at 30 °C. Reactions were stopped by the addition of SDS (1% final) and EDTA (1 mM final). Stopped reactions were analyzed by electrophoresis through 1.2% (w/v) agarose gels with 0.5X TBE running buffer. Gels were run at 2 V/cm for 12–18 hours, stained with ethidium bromide (EtBr), and visualized by UV illumination. To corroborate the findings from enzyme titrations, time-course assays were run with constant amounts of protein (data not shown).

To determine relative activities of topo IV enzymes on different substrates, we quantified the amounts of supercoiled and relaxed DNA in each lane using ImageJ.[76] First we divided each lane into two zones corresponding to "supercoiled" and "relaxed," with the split halfway between the most supercoiled and relaxed species. Next, we corrected for background staining and the different staining intensity of supercoiled *versus* relaxed DNA, and plotted the percent of relaxed/decatenated DNA *versus* enzyme concentration. Fitting these points allowed us to estimate the amount of enzyme needed to achieve "half-relaxation," and thus determine a rough measure of specific activity. These measures are to some extent approximate, but should be internally consistent for the purposes of comparison. For the graph in Figure 5(d), all specific activities are normalized to that of CTD-truncated topo IV on negatively supercoiled DNA.

Topo IV DNA binding assays

Purified negatively supercoiled pSG483 was linearized with BamHI (NEB), radiolabeled with T4 polynucleotide kinase in the presence of [γ-^{32}P]ATP (3000 μCi/mmol), and separated from unincorporated nucleotides using a spin column (BioRad; Biogel P-30). Filter binding was carried out using a Schleicher and Schuell 96-well Minifold dot-blot apparatus. Whatman filter paper and nitrocellulose and Nytran membranes (Schleicher and Schuell) were wet briefly in water, then soaked in wash buffer (25 mM Tris–HCl (pH 7.5), 20 mM NaCl, 10 mM $MgCl_2$, 1 mM EDTA, 10 mM β-mercaptoethanol). Two Whatman filters, the Nytran membrane, and the nitrocellulose membrane were placed, in that order, on the Minifold apparatus.

Binding reactions (160 μl) were carried out in binding buffer (25 mM Tris–HCl (pH 7.6 at 30 °C), 13 mM NaCl, 6 mM KCl, 10 mM $MgCl_2$, 2 mM DTT, 50 μg/ml BSA). Varying amounts of reconstituted topo IV were incubated with 0.5 nM ^{32}P-labeled linearized pSG483 for 30 minutes at 30 °C, then three 50 μl aliquots were added to separate 350 μl aliquots of binding buffer. Reaction mixtures were passed through the filters, then each well was washed three times with 450 μl of wash buffer and membranes were removed from the apparatus and dried. Dried filters were exposed to a BioRad imaging screen, then scanned using a Typhoon 8600 imager (Amersham Biosciences). The amounts of DNA bound at each spot were quantified by densitometry (ImageQuant). Total DNA amounts for each well were determined by summing the densities of spots on the nitrocellulose (protein–DNA complex) and Nytran (free DNA) filters. The fraction of DNA bound to protein was plotted *versus* protein (heterotetramer) concentration using KaleidaGraph (Synergy Software) and fit to an independent-sites binding model:[77]

$$\left(\alpha = \alpha_M \frac{([P]_T + [DNA]_T + K_d(app)) - (([P]_T + [DNA]_T + K_d(app))^2 - 4[P]_T[DNA]_r)^{0.5}}{2[DNA]_T}\right)$$

where α is the percentage of DNA bound, α_M is the percentage of DNA bound at saturation, $[P]_T$ is the total protein concentration, $[DNA]_T$ is the total concentration of DNA and K_d(app) is the apparent dissociation constant.

Sequence alignments

All annotated bacterial GyrA and ParC sequences (as of March 2004) were downloaded from TIGR†. In cases

† www.tigr.org

where multiple annotations disagreed in terms of gene length, the TIGR annotated version was used. Sequences were aligned using CLUSTALX,[78] and an unrooted phylogenetic tree was generated using DRAWTREE from the PHYLIP software package.[79]

Coordinates

The coordinates of the two structures have been deposited in the RCSB Protein Data Bank under accession numbers 1ZVT (ParC CTD) and 1ZVU (ParC27).

Acknowledgements

The authors thank J. Holton, J. Tanamachi, and G. Meigs for assistance at ALS Beamline 8.3.1; S. Gradia for supplying plasmid pSG483; A. McClendon and N. Osheroff for assistance with the preparation of positively supercoiled DNA; and D. Classen, J. Erzberger, N. Crisona, N. Cozzarelli, and H. Hiasa for helpful discussions and valuable assistance. K.D.C. & A.J.S. acknowledge support from NSF Graduate Research Fellowships, and J.M.B. acknowledges support from the NIH (CA 77373).

Supplementary Data

Supplementary data associated with this article can be found, in the online version, at doi:10.1016/j.jmb.2005.06.029

References

1. Postow, L., Crisona, N. J., Peter, B. J., Hardy, C. D. & Cozzarelli, N. R. (2001). Topological challenges to DNA replication: conformations at the fork. *Proc. Natl Acad. Sci. USA*, **98**, 8219–8226.
2. Gamper, H. B. & Hearst, J. E. (1982). A topological model for transcription based on unwinding angle analysis of *E. coli* RNA polymerase binary, initiation and ternary complexes. *Cell*, **29**, 81–90.
3. Liu, L. F. & Wang, J. C. (1987). Supercoiling of the DNA template during transcription. *Proc. Natl Acad. Sci. USA*, **84**, 7024–7027.
4. Mizuuchi, K., Gellert, M., Weisberg, R. A. & Nash, H. A. (1980). Catenation and supercoiling in the products of bacteriophage lambda integrative recombination *in vitro*. *J. Mol. Biol.* **141**, 485–494.
5. Wasserman, S. A. & Cozzarelli, N. R. (1986). Biochemical topology: applications to DNA recombination and replication. *Science*, **232**, 951–960.
6. Hardy, C. D., Crisona, N. J., Stone, M. D. & Cozzarelli, N. R. (2004). Disentangling DNA during replication: a tale of two strands. *Phil. Trans. Roy. Soc. ser. B*, **359**, 39–47.
7. Corbett, K. D. & Berger, J. M. (2004). Structure, molecular mechanisms, and evolutionary relationships in DNA topoisomerases. *Annu. Rev. Biophys. Biomol. Struct.* **33**, 95–118.
8. Wang, J. C. (1998). Moving one DNA double helix through another by a type II DNA topoisomerase: the story of a simple molecular machine. *Quart. Rev. Biophys.* **31**, 107–144.
9. Champoux, J. J. (2001). DNA topoisomerases: structure, function, and mechanism. *Annu. Rev. Biochem.* **70**, 369–413.
10. Wang, J. C. (2002). Cellular roles of topoisomerases: a molecular perspective. *Nature Rev. Mol. Cell. Biol.* **3**, 430–440.
11. Zechiedrich, E. L., Khodursky, A. B., Bachellier, S., Schneider, R., Chen, D., Lilley, D. M. & Cozzarelli, N. R. (2000). Roles of topoisomerases in maintaining steady-state DNA supercoiling in *Escherichia coli*. *J. Biol. Chem.* **275**, 8103–8113.
12. Funnell, B. E., Baker, T. A. & Kornberg, A. (1987). *In vitro* assembly of a prepriming complex at the origin of the *Escherichia coli* chromosome. *J. Biol. Chem.* **262**, 10327–10334.
13. Marians, K. J., Minden, J. S. & Parada, C. (1986). Replication of superhelical DNAs *in vitro*. *Prog. Nucl. Acid Res. Mol. Biol.* **33**, 111–140.
14. Pruss, G. J. & Drlica, K. (1989). DNA supercoiling and prokaryotic transcription. *Cell*, **56**, 521–523.
15. Peter, B. J., Arsuaga, J., Breier, A. M., Khodursky, A. B., Brown, P. O. & Cozzarelli, N. R. (2004). Genomic transcriptional response to loss of chromosomal supercoiling in *Escherichia coli*. *Genome Biol.* **5**, R87.
16. Zechiedrich, E. L. & Cozzarelli, N. R. (1995). Roles of topoisomerase IV and DNA gyrase in DNA unlinking during replication in *Escherichia coli*. *Genes Dev.* **9**, 2859–2869.
17. Adams, D. E., Shekhtman, E. M., Zechiedrich, E. L., Schmid, M. B. & Cozzarelli, N. R. (1992). The role of topoisomerase IV in partitioning bacterial replicons and the structure of catenated intermediates in DNA replication. *Cell*, **71**, 277–288.
18. Kato, J., Nishimura, Y., Imamura, R., Niki, H., Hiraga, S. & Suzuki, H. (1990). New topoisomerase essential for chromosome segregation in *E. coli*. *Cell*, **63**, 393–404.
19. Gellert, M., Mizuuchi, K., O'Dea, M. H. & Nash, H. A. (1976). DNA gyrase: an enzyme that introduces superhelical turns into DNA. *Proc. Natl Acad. Sci. USA*, **73**, 3872–3876.
20. Liu, L. F. & Wang, J. C. (1978). *Micrococcus luteus* DNA gyrase: active components and a model for its supercoiling of DNA. *Proc. Natl Acad. Sci. USA*, **75**, 2098–2102.
21. Mizuuchi, K., O'Dea, M. H. & Gellert, M. (1978). DNA gyrase: subunit structure and ATPase activity of the purified enzyme. *Proc. Natl Acad. Sci. USA*, **75**, 5960–5963.
22. Huang, W. M. (1996). Bacterial diversity based on type II DNA topoisomerase genes. *Annu. Rev. Genet.* **30**, 79–107.
23. Marians, K. J. (1987). DNA gyrase-catalyzed decatenation of multiply linked DNA dimers. *J. Biol. Chem.* **262**, 10362–10368.
24. Ullsperger, C. & Cozzarelli, N. R. (1996). Contrasting enzymatic activities of topoisomerase IV and DNA gyrase from *Escherichia coli*. *J. Biol. Chem.* **271**, 31549–31555.
25. Reece, R. J. & Maxwell, A. (1991). The C-terminal domain of the *Escherichia coli* DNA gyrase A subunit is a DNA-binding protein. *Nucl. Acids Res.* **19**, 1399–1405.
26. Kampranis, S. C. & Maxwell, A. (1996). Conversion of DNA gyrase into a conventional type II topoisomerase. *Proc. Natl Acad. Sci. USA*, **93**, 14416–14421.
27. Corbett, K. D., Shultzaberger, R. K. & Berger, J. M.

(2004). The C-terminal domain of DNA gyrase A adopts a DNA-bending β-pinwheel fold. *Proc. Natl Acad. Sci. USA*, **101**, 7293–7298.
28. Ruthenburg, A. J., Graybosch, D. M., Huetsch, J. C. & Verdine, G. L. (2005). A superhelical spiral in the *Escherichia coli* DNA gyrase A C-terminal domain imparts unidirectional supercoiling bias. *J. Biol. Chem.* In the press.
29. Vologodskii, A. (2004). Computational analysis of DNA gyrase action. *Biophys. J.* **87**, 3066–3073.
30. Brown, P. O. & Cozzarelli, N. R. (1979). A sign inversion mechanism for enzymatic supercoiling of DNA. *Science*, **206**, 1081–1083.
31. Peng, H. & Marians, K. J. (1993). *Escherichia coli* topoisomerase IV. Purification, characterization, subunit structure, and subunit interactions. *J. Biol. Chem.* **268**, 24481–24490.
32. Espeli, O., Lee, C. & Marians, K. J. (2003). A physical and functional interaction between *Escherichia coli* FtsK and topoisomerase IV. *J. Biol. Chem.* **278**, 44639–44644.
33. Huang, W. M., Libbey, J. L., van der Hoeven, P. & Yu, S. X. (1998). Bipolar localization of *Bacillus subtilis* topoisomerase IV, an enzyme required for chromosome segregation. *Proc. Natl Acad. Sci. USA*, **95**, 4652–4657.
34. Wang, S. C. & Shapiro, L. (2004). The topoisomerase IV ParC subunit colocalizes with the *Caulobacter* replisome and is required for polar localization of replication origins. *Proc. Natl Acad. Sci. USA*, **101**, 9251–9256.
35. Crisona, N. J., Strick, T. R., Bensimon, D., Croquette, V. & Cozzarelli, N. R. (2000). Preferential relaxation of positively supercoiled DNA by *E. coli* topoisomerase IV in single-molecule and ensemble measurements. *Genes Dev.* **14**, 2881–2892.
36. Stone, M. D., Bryant, Z., Crisona, N. J., Smith, S. B., Vologodskii, A. V., Bustamante, C. & Cozzarelli, N. R. (2003). Chirality sensing by *Escherichia coli* topoisomerase IV and the mechanism of type II topoisomerases. *Proc. Natl Acad. Sci. USA*, **100**, 8654–8659.
37. Charvin, G., Bensimon, D. & Croquette, V. (2003). Single-molecule study of DNA unlinking by eukaryotic and prokaryotic type-II topoisomerases. *Proc. Natl Acad. Sci. USA*, **100**, 9820–9825.
38. Peng, H. & Marians, K. J. (1995). The interaction of *Escherichia coli* topoisomerase IV with DNA. *J. Biol. Chem.* **270**, 25286–25290.
39. Hsieh, T.-J., Farh, L., Huang, W. M. & Chan, N. L. (2004). Structure of the topoisomerase IV C-terminal domain: a broken β-propeller implies a role as geometry facilitator in catalysis. *J. Biol. Chem.* **279**, 55587–55593.
40. Ward, D. & Newton, A. (1997). Requirement of topoisomerase IV parC and parE genes for cell cycle progression and developmental regulation in *Caulobacter crescentus*. *Mol. Microbiol.* **26**, 897–910.
41. Morais Cabral, J. H., Jackson, A. P., Smith, C. V., Shikotra, N., Maxwell, A. & Liddington, R. C. (1997). Crystal structure of the breakage-reunion domain of DNA gyrase. *Nature*, **388**, 903–906.
42. Berger, J. M., Gamblin, S. J., Harrison, S. C. & Wang, J. C. (1996). Structure and mechanism of DNA topoisomerase II. *Nature*, **379**, 225–232.
43. Fass, D., Bogden, C. E. & Berger, J. M. (1999). Quaternary changes in topoisomerase II may direct orthogonal movement of two DNA strands. *Nature Struct. Biol.* **6**, 322–326.
44. Kirchhausen, T., Wang, J. C. & Harrison, S. C. (1985). DNA gyrase and its complexes with DNA: direct observation by electron microscopy. *Cell*, **41**, 933–943.
45. Costenaro, L., Grossmann, J. G., Ebel, C. & Maxwell, A. (2005). Small-angle X-ray scattering reveals the solution structure of the full-length DNA gyrase A subunit. *Structure*, **13**, 287–295.
46. Ikura, M., Clore, G. M., Gronenborn, A. M., Zhu, G., Klee, C. B. & Bax, A. (1992). Solution structure of a calmodulin–target peptide complex by multidimensional NMR. *Science*, **256**, 632–638.
47. Keenan, R. J., Freymann, D. M., Walter, P. & Stroud, R. M. (1998). Crystal structure of the signal sequence binding subunit of the signal recognition particle. *Cell*, **94**, 181–191.
48. Kreuzer, K. N. & Cozzarelli, N. R. (1980). Formation and resolution of DNA catenanes by DNA gyrase. *Cell*, **20**, 245–254.
49. Marini, J. C., Miller, K. G. & Englund, P. T. (1980). Decatenation of kinetoplast DNA by topoisomerases. *J. Biol. Chem.* **255**, 4976–4979.
50. Shapiro, T. A. & Englund, P. T. (1995). The structure and replication of kinetoplast DNA. *Annu. Rev. Microbiol.* **49**, 117–143.
51. Liu, L. F. & Wang, J. C. (1978). DNA–DNA gyrase complex: the wrapping of the DNA duplex outside the enzyme. *Cell*, **15**, 979–984.
52. Heddle, J. G., Mitelheiser, S., Maxwell, A. & Thomson, N. H. (2004). Nucleotide binding to DNA gyrase causes loss of DNA wrap. *J. Mol. Biol.* **337**, 597–610.
53. Fisher, L. M., Mizuuchi, K., O'Dea, M. H., Ohmori, H. & Gellert, M. (1981). Site-specific interaction of DNA gyrase with DNA. *Proc. Natl Acad. Sci. USA*, **78**, 4165–4169.
54. Klevan, L. & Wang, J. C. (1980). Deoxyribonucleic acid gyrase–deoxyribonucleic acid complex containing 140 base-pairs of deoxyribonucleic acid and an $\alpha_2\beta_2$ protein core. *Biochemistry*, **19**, 5229–5234.
55. Buck, G. R. & Zechiedrich, E. L. (2004). DNA disentangling by type-2 topoisomerases. *J. Mol. Biol.* **340**, 933–939.
56. Rybenkov, V. V., Ullsperger, C., Vologodskii, A. V. & Cozzarelli, N. R. (1997). Simplification of DNA topology below equilibrium values by type II topoisomerases. *Science*, **277**, 690–693.
57. Vologodskii, A. V., Zhang, W., Rybenkov, V. V., Podtelezhnikov, A. A., Subramanian, D., Griffith, J. D. & Cozzarelli, N. R. (2001). Mechanism of topology simplification by type II DNA topoisomerases. *Proc. Natl Acad. Sci. USA*, **98**, 3045–3049.
58. Manjunatha, U. H., Dalal, M., Chatterji, M., Radha, D. R., Visweswariah, S. S. & Nagaraja, V. (2002). Functional characterisation of mycobacterial DNA gyrase: an efficient decatenase. *Nucl. Acids Res.* **30**, 2144–2153.
59. Tortoli, E. (2003). Impact of genotypic studies on mycobacterial taxonomy: the new mycobacteria of the 1990s. *Clin. Microbiol. Rev.* **16**, 319–354.
60. Kapust, R. B. & Waugh, D. S. (1999). *Escherichia coli* maltose-binding protein is uncommonly effective at promoting the solubility of polypeptides to which it is fused. *Protein Sci.* **8**, 1668–1674.
61. Van Duyne, G. D., Standaert, R. F., Karplus, P. A., Schreiber, S. L. & Clardy, J. (1993). Atomic structures of the human immunophilin FKBP-12 complexes with FK506 and rapamycin. *J. Mol. Biol.* **229**, 105–124.
62. MacDowell, A. A., Celestre, R. S., Howells, M., McKinney, W., Krupnick, J., Cambie, D. *et al*. (2004). Suite of three protein crystallography beamlines with single superconducting bend magnet as the source. *J. Synchrotron Radiat.* **11**, 447–455.

63. Otwinowski, Z. & Minor, W. (1997). Processing of X-ray diffraction data collected in oscillation mode. *Methods Enzymol.* **276**, 472–494.
64. Holton, J. & Alber, T. (2004). Automated protein crystal structure determination using ELVES. *Proc. Natl Acad. Sci. USA*, **101**, 1537–1542.
65. Leslie, A. G. W. (1992). Recent changes to the MOSFLM package for processing film and image plate data. *Joint CCP4 +ESF-EAMCB Newsletter on Protein Crystallography*, **26**.
66. Terwilliger, T. (2004). SOLVE and RESOLVE: automated structure solution, density modification and model building. *J. Synchrotron. Radiat.* **11**, 49–52.
67. Collaborative Computational Project Number. (1994). The CCP4 suite: programs for protein crystallography. *Acta Crystallog. sect. D*, **50**, 760–763.
68. Jones, T. A. & Kjeldgaard, M. (1997). *O—The Manual, Version 7.0* 1997. Uppsala, Sweden.
69. Lamzin, V. S. & Wilson, K. S. (1993). Automated refinement of protein models. *Acta Crystallog. sect. D*, **49**, 129–147.
70. Winn, M. D., Isupov, M. N. & Murshudov, G. N. (2001). Use of TLS parameters to model anisotropic displacements in macromolecular refinement. *Acta Crystallog. sect. D*, **57**, 122–133.
71. Storoni, L. C., McCoy, A. J. & Read, R. J. (2004). Likelihood-enhanced fast rotation functions. *Acta Crystallog. sect. D*, **60**, 432–438.
72. Brunger, A. T., Adams, P. D., Clore, G. M., DeLano, W. L., Gros, P., Grosse-Kunstleve, R. W. *et al*. (1998). Crystallography and NMR system: a new software suite for macromolecular structure determination. *Acta Crystallog. sect. D*, **54**, 905–921.
73. Baker, N. A., Sept, D., Joseph, S., Holst, M. J. & McCammon, J. A. (2001). Electrostatics of nanosystems: application to microtubules and the ribosome. *Proc. Natl Acad. Sci. USA*, **98**, 10037–10041.
74. DeLano, W. L. (2002). *PyMOL*, DeLano Scientific, San Carlos, CA.
75. Rodriguez, A. C. (2002). Studies of a positive supercoiling machine: nucleotide hydrolysis and a multifunctional latch in the mechanism of reverse gyrase. *J. Biol. Chem.* **277**, 29865–29873.
76. Rasband, W. S. (1997–2005). *ImageJ*, US National Institutes of Health, Bethesda, MD.
77. Clarke, A. R. (1996). In *Enzymology, Labfax* (Engel, P. C., ed.), chapter 6. BIOS Scientific Publishers and Academic Press, San Diego, CA, USA.
78. Jeanmougin, F., Thompson, J. D., Gouy, M., Higgins, D. G., Gibson, T. & J, . (1998). Multiple sequence alignment with Clustal X. *Trends. Biochem. Sci.* **23**, 403–405.
79. Felsenstein, J. (2004). *PHYLIP (Phylogeny Inference Package) version 3.6*, Department of Genome Sciences, University of Washington, Seattle.
80. Jones, D. T. (1999). Protein secondary structure prediction based on position-specific scoring matrices. *J. Mol. Biol.* **292**, 195–202.

Edited by J. Doudna

(Received 27 April 2005; received in revised form 9 June 2005; accepted 10 June 2005)
Available online 28 June 2005